Available online at www.sciencedirect.com

SciVerse ScienceDirect

Acta Materialia 60 (2012) 2135–2145

Acta MATERIALIA

www.elsevier.com/locate/actamat

# Crystal plasticity modeling of texture development and hardening in TWIP steels

S. Dancette [a], L. Delannay [a,*], K. Renard [b], M.A. Melchior [a], P.J. Jacques [b]

[a] Department of Mechanical Engineering (MEMA), Université Catholique de Louvain (UCL), Av. G. Lemaitre 4, 1348 Louvain-la-Neuve, Belgium
[b] Department of Materials Sciences and Processes (IMAP), Université Catholique de Louvain (UCL), Place Sainte Barbe 2, 1348 Louvain-la-Neuve, Belgium

Received 26 September 2011; received in revised form 21 December 2011; accepted 10 January 2012

**Abstract**

A new crystal plasticity model for face-centered cubic metals exhibiting deformation twinning is presented and assessed based on a comprehensive and original experimental dataset for twinning-induced plasticity (TWIP) steel. Various scale transition schemes are tested, including a finite-element representation of the polycrystalline aggregate and a simplified Taylor-type modeling of pairwise interactions of adjacent grains. The same constitutive law is used at the grain level, relying on a dislocation-density-based description of work hardening and accounting for the latent hardening due to the presence of twins. At the macroscopic scale, the model provides improved predictions of the development of texture and hardening in uniaxial tension and during rolling. At the grain level, electron backscatter diffraction measurements confirm that the model properly estimates the volume fraction of twins inside individual grains as well as the average disorientation relative to the grain mean lattice orientation.


*Keywords:* Crystal plasticity; Multisite model; Finite elements; fcc Materials; Twinning

## 1. Introduction

The acronym TWIP stands for "TWinning-Induced Plasticity". It refers to a substantial increase in the hardening capacity and ductility of austenitic steel grades in which a dynamic Hall–Petch effect occurs due to the formation of thin (<100 nm) mechanical twins acting as obstacles to dislocation glide [1–4]. In comparison with hexagonal closed-packed (hcp) alloys, face-centered cubic (fcc) metals, such as TWIP steels, produce low volume fractions of twins (typically less than 30%). Nevertheless, the influence of twinning on the mechanical response is significant and often underestimated by crystal plasticity models. Physically sound predictions of the macroscopic strain hardening and induced anisotropy (texture development) require, on the one hand, a proper modeling of the interplay of twinning and dislocation slip within individual grains and, on the other hand, a valid (and computationally affordable) scale transition scheme.

The so-called "copper-to-brass transition" of cold rolling textures in fcc metals is probably the most debated effect of twinning to date. Nowadays, the most widespread explanation is summarized as follows [5]: (i) within each grain, dislocation slip occurs predominantly along the most stressed $\langle 1\,1\,1\rangle$ plane because twin lamellae formed parallel to this plane hinder dislocation motion along other slip planes; (ii) adjacent grains adopt heterogeneous and geometrically compatible deformation patterns; (iii) after large strains, plastic localization into shear bands may "unlock" regions where two sets of twin lamellae intersect and tend to impede further uniform deformation. Successful texture predictions require large strain heterogeneity from one grain to another as demonstrated by the viscoplastic self-consistent (VPSC) scheme [6]. This scheme was applied to Hadfield steels (similar to TWIP steels) by Karaman

* Corresponding author.
*E-mail address:* laurent.delannay@uclouvain.be (L. Delannay).

1359-6454/$36.00 © 2012 Acta Materialia Inc. Published by Elsevier Ltd. All rights reserved.
doi:10.1016/j.actamat.2012.01.015

et al. [2] who focused on the deformation behavior of single crystals and polycrystals in uniaxial tension. Also noteworthy is the composite grain model of Proust et al. [7] who enriched the VPSC scheme in order to account for the co-deformation of twin lamellae and parent grain (in hcp metals).

Twinning contributes to the macroscopic hardening of TWIP steels in two different ways. First, the evolving inter-twin distance reduces the mean free path of mobile dislocations in the parent grain. The resulting dislocation storage and hardening of fcc metals has been considered by various authors [2,8–10]. Allain et al. [3] and Shiekhelsouk et al. [11] accounted for the anisotropy of slip–twin and slip–slip interactions and the latent hardening effect on the slip system selection. Similar strategies were developed in case of hcp alloys [7,12]. A second contribution to macroscopic hardening was highlighted by Gil Sevillano [13], who estimated the very high stresses developing inside the thin twin lamellae where plasticity is highly constrained. Twinned regions may thus be seen as very hard inclusions leading to a composite type of hardening.

In order to account for the latter two hardening contributions, the present work relies on the total Lagrangian framework due to Kalidindi [9,14]. However, unlike the latter original studies, the present model accounts for the heterogeneity of deformation throughout the polycrystalline aggregate. Two scale transition schemes, other than the isostrain assumption and the VPSC model, are tested here. The first one is the crystal-plasticity-based finite-element method (CPFEM) allowing full-field calculations over large samplings of grains constituting representative volume elements (RVEs) of the microstructure and texture (e.g. [15–17]). The second scale transition scheme is called the multisite model. It is an elastic–viscoplastic extension of the ALAMEL model [18]. The latter was originally meant only for the prediction of rolling textures. The multisite model considers that each grain interacts preferentially with one neighbor across a planar, "sticking" interface. The local heterogeneity of strain is predicted by minimizing the deformation energy of the two grains (as further explained below). The multisite model has, for instance, provided reliable quantitative predictions of planar anisotropy in textured steel sheets [19]. However, neither the ALAMEL model nor the multisite model were ever applied to alloys undergoing mechanical twinning. This is done here while relying on the hardening law of Shiekhelsouk et al. [11] at the single-crystal level. Such crystal plasticity law is also implemented in the Abaqus finite-element code allowing full-field CPFEM throughout the polycrystalline aggregate.

In addition to the model development, the present study comprises an extensive experimental investigation of a Fe–20% Mn–1.2% C TWIP steel. In order to calibrate and then assess the model, two loading modes have been considered: rolling and uniaxial tension. Strain hardening has been measured during tensile tests performed on samples with and without pre-strain by rolling. The macroscopic texture development has been probed by X-ray diffraction (XRD), whereas careful orientation mapping by electron back-scatter diffraction (EBSD) has provided estimates of the evolving twin volume fraction (TVF) and the microtexture (e.g. the evolving twin-to-parent lattice disorientation). The latter observations, which stem from large, statistically representative samplings of the microstructure, where also compared to a recent, high-resolution investigation of the same alloy by transmission electron microscopy [20,21]. Such comprehensive experimental study performed on a single TWIP grade is seldom found in the literature.

The paper is organized as follows: the model is briefly described in Section 2, then predictions are assessed in Section 3 at the macroscopic level and at the grain level. These results are discussed in Section 4, leading to the final conclusions.

## 2. Model

### 2.1. Single grain crystal plasticity

The present modeling framework considers twins as individual crystal entities and keeps track of the evolving orientation relationship between a parent grain and its twins. The twin volume fraction produced inside each grain will be used in Section 3 for the assessment of the model at the grain level.

The Cauchy stress $\boldsymbol{\sigma}$ developed within each crystal and the rate of twinning are predicted based on the usual, multiplicative decomposition of the deformation gradient tensor $\boldsymbol{F} = \boldsymbol{R}^* \boldsymbol{U}^{el} \boldsymbol{F}^p$, where $\boldsymbol{R}^*$ is the lattice rotation, $\boldsymbol{U}^{el} = \mathbf{1} + \boldsymbol{\epsilon}^{el}$ an infinitesimal elastic stretch, and $\boldsymbol{F}^p$ the mapping as a result of dislocation slip and twinning. The velocity gradient tensor $\boldsymbol{L}$ is:

$$\boldsymbol{L} = \dot{\boldsymbol{F}}\boldsymbol{F}^{-1} \simeq \dot{\boldsymbol{R}}^* \boldsymbol{R}^{*T} + \boldsymbol{R}^* (\dot{\boldsymbol{\epsilon}}^{el} + \boldsymbol{L}^p) \boldsymbol{R}^{*T} \tag{1}$$

where

$$\boldsymbol{L}^p = \dot{\boldsymbol{F}}^p \boldsymbol{F}^{p-1} = \sum_g \boldsymbol{M}^g \dot{\gamma}^g + \sum_h \boldsymbol{M}^h \dot{\gamma}^h \tag{2}$$

Here, $\boldsymbol{M}^g = \boldsymbol{b}^g \otimes \boldsymbol{n}^g$ and $\boldsymbol{M}^h = \boldsymbol{b}^h \otimes \boldsymbol{n}^h$ are the Schmid tensors on the slip system $g$ and twin system $h$, respectively, $\boldsymbol{b}^g$, $\boldsymbol{b}^h$ are normalized Burgers vectors, and $\boldsymbol{n}^g$, $\boldsymbol{n}^h$ are the normals to the slip and twinning planes. Dislocation slip occurs along 12 $\{1\,1\,1\}\langle 1\,1\,0\rangle$ slip systems whereas 12 $\{1\,1\,1\}\langle 1\,1\,2\rangle$ twin systems are considered. The shear rates are computed using a viscoplastic power-law [22]:

$$\begin{aligned} \dot{\gamma}^g &= \dot{\gamma}_0 \left| \frac{\boldsymbol{M}^g : \tilde{\boldsymbol{\sigma}}}{\tau_c^g} \right|^{1/m} sign(\boldsymbol{M}^g : \tilde{\boldsymbol{\sigma}}) \\ \dot{\gamma}^h &= \dot{\gamma}_0 \left( \frac{\boldsymbol{M}^h : \tilde{\boldsymbol{\sigma}}}{\tau_c^h} \right)^{1/m} \quad \text{if} \quad \boldsymbol{M}^h : \tilde{\boldsymbol{\sigma}} > 0 \end{aligned} \tag{3}$$

$\dot{\gamma}_0 = 0.001/\mathrm{s}$ is a reference slip rate, $m = 0.05$ is the rate sensitivity exponent and $\tau_c^{g \text{ or } h}$ are the critical resolved shear stresses (CRSSs) according to the generalized Schmid law. $\tilde{\boldsymbol{\sigma}}$ is the second Piola–Kirchhoff stress computed in the intermediate configuration defined by a mapping through

$\boldsymbol{F}\boldsymbol{F}^{p-1} = \boldsymbol{R}^*\boldsymbol{U}^{el}$. Using the elastic stiffness $C$ and the assumption of infinitesimal elastic stretches, we have:

$$C : \dot{\boldsymbol{\epsilon}}^{el} = \dot{\tilde{\boldsymbol{\sigma}}} = det(\boldsymbol{F})\ \boldsymbol{U}^{el\,-1}\boldsymbol{R}^{*\mathrm{T}}\dot{\boldsymbol{\sigma}}\ \boldsymbol{R}^*\boldsymbol{U}^{el\,-1} \simeq \boldsymbol{R}^{*\mathrm{T}}\ \dot{\boldsymbol{\sigma}}\ \boldsymbol{R}^* \quad (4)$$

$\boldsymbol{R}^*$ is obtained by time integration of the skew-symmetric part of Eq. (1). This applies separately to both the parent grains and the twins. Time integration is fully implicit, except for the evaluation of the twin volume fraction. In fcc metals, each twin formation implies a local shear of amplitude $1/\sqrt{2}$. During a time step, the amplitude of shear due to twinning is $\dot{\gamma}^h\Delta t$. Hence, a volume $\Delta f^h = \sqrt{2}\dot{\gamma}^h\Delta t$ is transferred from the parent grain to the twin at the end of each time step. No secondary twinning is allowed in existing twins, in agreement with previous experimental observations (e.g. [23]).

The stress in a grain is computed as a volumetric average of the stresses in the parent grain and the twins. Uniform deformation is assumed between them, which was also assumed by Kalidindi [14]. This can be motivated by the necessary compatibility of deformation between the twin lamellae and the parent grain [13].

Anisotropic hardening of the crystals is considered and a distinction is made between the resistance to dislocation slip in the parent grain, the resistance to twinning in the parent grain and the resistance to slip inside existing twins.

*Deformation by slip in the parent grain*. Inspired from the work of Allain et al. [3] and Shielhelsouk et al. [11], strain hardening here is directly related to the mean free path (MFP) of dislocations, $\Lambda^g$, measured along each slip system. $\Lambda^g$ depends on the grain diameter $D$, the density of forest dislocations $\rho$ and the intertwin distance $T^g$. The latter is specific to each slip system and decreases when the twin volume fraction is increased:

$$\frac{1}{\Lambda^g} = \frac{1}{D} + \frac{1}{T^g} + \frac{\sqrt{\sum_{i\neq g}\rho^i}}{K} \quad (5)$$

$K$ measures the resistance of the forest of dislocations and, based on Fulmann's volumetric analysis [1],

$$\frac{1}{T^g} = \sum_h B^{gh}\frac{f^h}{2re\left(1-\sum_1^{12} f^h\right)}. \quad (6)$$

Here, $f^h$ is the volume fraction of twin lamellae of system $h$, $e$ is the twin thickness, $r$ is the number of twins in each bundle and $B$ is a slip–twin interaction matrix where $B^{gh} = 0$ if slip system $g$ and twin system $h$ are coplanar; otherwise $B^{gh} = 1$.

The rate of increase of the dislocation density stored in a slip system, $\dot{\rho}^g$, is proportional to the slip rate along the same system [24]:

$$\dot{\rho}^g = \frac{1}{b_{110}}\left(\frac{1}{\Lambda^g} - \beta\rho^g\right)|\dot{\gamma}^g| \quad (7)$$

where $b_{110}$ is the Burgers vector for $\{1\,1\,1\}\langle 1\,1\,0\rangle$ slip and $-\beta\rho^g$ is a recovery term.

Finally, assuming Taylor hardening and adopting Franciosi's approach for multiple slip systems [25], we obtain:

$$\tau_c^g = \tau_{c0}^g + \alpha\mu b_{110}\sqrt{\sum_k A^{gk}\rho^k} \quad (8)$$

$\tau_{c0}^g$ here is the initial shear strength, $\alpha$ characterizes the resistance of the forest, $\mu$ is the shear modulus of the material and $A^{gk}$ is a slip–slip interaction matrix. Differentiating $\tau_c^g$ with respect to time and substituting Eq. (7) yields:

$$\dot{\tau}_c^g = \sum_k H^{gk}|\dot{\gamma}^k| \quad (9)$$

where

$$H^{gk} = \frac{\alpha\mu}{2\sqrt{\sum_l A^{gl}\rho^l}} A^{gk}\left(\frac{1}{\Lambda^k} - \beta\rho^k\right) \quad (10)$$

*Deformation by slip in existing twins*. A similar modeling of work hardening holds inside the twins. However, the dislocation MFP is now a function of only the twin geometry and the dislocation density stored within the twins (secondary twinning is forbidden):

$$\frac{1}{\Lambda^g} = \frac{1}{\sqrt{reD}} + \frac{\sqrt{\sum_{i\neq g}\rho^i}}{K} \quad (11)$$

*Deformation by twinning in the parent grain*. Twinning kinetics results from rather intricate mechanisms regarding the formation of twin nuclei and their subsequent growth within a crystal containing dislocations as well as other twins (e.g. [20,21] in TWIP steels and Beyerlein and Tomé [12] in hcp materials). The present work relies on a heuristic hardening law proposed by Kalidindi (e.g. [9,11]):

$$\dot{\tau}_c^h = H_{ncp}\left(\sum_k f^k\right)^b \sum_{k\in ncp}\dot{\gamma}^k + H_{cp}\left(\sum_k f^k\right)\sum_{k\in cp}\dot{\gamma}^k \quad (12)$$

In this expression, subscripts *cp* and *ncp* refer the sets of twin systems which are, respectively, coplanar and non-coplanar with the twin system $h$. The parameters $H_{ncp}$ and $H_{cp}$ and the $b$ exponent are adjusted in such a way as to favor twinning along only the most highly stressed $\{1\,1\,1\}$ plane, as observed experimentally at low levels of deformation. After larger strains, when other twin systems become active, the twin volume fraction tends to saturate. Dislocation slip activity is not taken into account. It is assumed that its influence is small in comparison with the influence of twinning itself [9].

### 2.2. Scale transition

The deformation of individual grains still remains to be defined since it is different from the known macroscopic deformation. Two homogenization schemes are proposed here. From a computational viewpoint, the first one is much less demanding than the second.

The so-called multisite model is an elastic–viscoplastic extension of the ALAMEL model developed by Van Houtte et al. [18]. Whereas other mean field approaches, such as the well-known VPSC model [26], focus on long-range interactions of the grains across the polycrystal, the

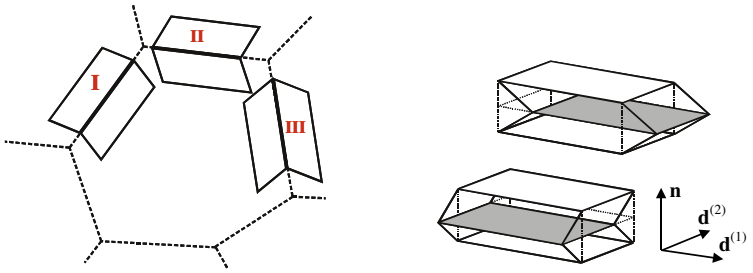


(a) Clusters of two interacting subregions

(b) Shear relaxations parallel to the interface

Fig. 1. Illustration of the multisite model of short-range grain interaction [19].

multisite model assumes instead that each grain interacts exclusively with its direct neighbors. We consider clusters of two (sub) grains separated by a planar interface (Fig. 1a). Stress balance across the interface is achieved by allowing some heterogeneity of strain. In supplement to the macroscopic strain, the two subregions undergo opposite shear parallel to the grain boundary. The velocity gradient tensors of the two subregions are then expressed by:

$$\boldsymbol{L}^{I} = \boldsymbol{L}^{macro} + \dot{\gamma}^{(1)}(\boldsymbol{d}^{(1)} \otimes \boldsymbol{n}) + \dot{\gamma}^{(2)}(\boldsymbol{d}^{(2)} \otimes \boldsymbol{n}) \tag{13}$$

$$\boldsymbol{L}^{II} = \boldsymbol{L}^{macro} - \dot{\gamma}^{(1)}(\boldsymbol{d}^{(1)} \otimes \boldsymbol{n}) - \dot{\gamma}^{(2)}(\boldsymbol{d}^{(2)} \otimes \boldsymbol{n}) \tag{14}$$

where $\boldsymbol{d}^{(1)}$ and $\boldsymbol{d}^{(2)}$ are arbitrary directions in the plane of the interface, and $\boldsymbol{n}$ is the interface normal (Fig. 1b). Hence, heterogeneity of strain is averaged out over every cluster of two subregions. The amplitude of shear, represented by $\dot{\gamma}^{(1)}$ and $\dot{\gamma}^{(2)}$, is computed by minimizing the deformation energy of the two subregions. This is approximately fulfilled by requiring that:

$$(\boldsymbol{\sigma}^{I} - \boldsymbol{\sigma}^{II}) : (\boldsymbol{d}^{(1)} \otimes \boldsymbol{n}) = (\boldsymbol{\sigma}^{I} - \boldsymbol{\sigma}^{II}) : (\boldsymbol{d}^{(2)} \otimes \boldsymbol{n}) = 0 \tag{15}$$

where $\boldsymbol{\sigma}^{I}$ and $\boldsymbol{\sigma}^{II}$ represent the Cauchy stresses of the two subregions.

The lattice disorientation of adjacent grains is assumed to be random. Starting from a large sampling of grain orientations representative of the initial texture [27], the lattice orientations of the subregions are randomly selected and associated in pairs at the onset of the simulation.

The orientation of the planar interface is different for each cluster. The interface normals $\boldsymbol{n}$ are statistically representative of the average grain shape. They are generated by randomly distributing the clusters on a surface defining the initial grain shape. For instance, in case of an ellipsoid with principal diameters $a$, $b$ and $c$, a normalized vector $\hat{\boldsymbol{x}}$ is generated randomly for each cluster and the interface normal is computed as:

$$\hat{\boldsymbol{n}} = \left(\frac{\hat{x}_1}{a^2}, \frac{\hat{x}_2}{b^2}, \frac{\hat{x}_3}{c^2}\right) \Big/ \sqrt{\left(\frac{\hat{x}_1}{a^2}\right)^2 + \left(\frac{\hat{x}_2}{b^2}\right)^2 + \left(\frac{\hat{x}_3}{c^2}\right)^2} \tag{16}$$

As the material deforms, the interface normal is updated according to the macroscopic deformation gradient: $\boldsymbol{n} = (\boldsymbol{F}^{-1})^{T} : \hat{\boldsymbol{n}}$.

CPFEM allows a more rigorous, and presumably more accurate, treatment of the scale transition. It produces full-field solutions of the deformation throughout a RVE of the polycrystalline aggregate (see the recent overview by Roters et al. [16]). Each grain is discretized into a large number of elements and integration points (with identical initial lattice orientation). Each integration point behaves as a single crystal subjected to finite strain increments. The crystal plasticity framework introduced above is implemented as a (fully implicit) user-defined material law in the Abaqus finite-element code.

As a compromise between accuracy and computational cost, grains are here represented by truncated octahedrons with 128 integration points [28]. Periodic boundary conditions are prescribed at the boundaries of a RVE containing 1024 grains, the lattice orientations of which reproduce the initial texture (Fig. 2).

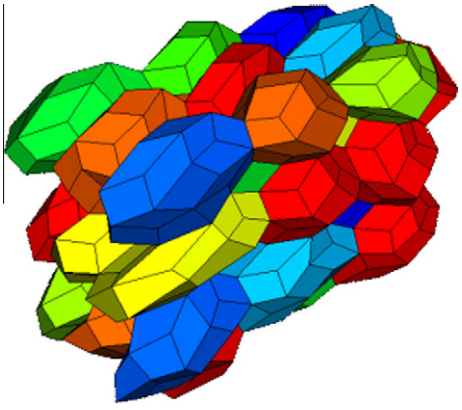

Fig. 2. Illustration of a deformed FEM mesh with grains shaped as truncated octahedrons [28]. The mesh used in the present analysis contains 1024 grains instead of 54 as is represented here.

## 3. Results

The alloy under consideration is a cold-rolled, 1.5 mm thick sheet made of Fe–20 wt.% Mn–1.2 wt.% C TWIP steel. It was annealed for 8 min at 950 °C prior to mechanical testing [21,29]. The initial (recrystallized) texture was measured by XRD and then discretized into 1000 orientations

Table 1
Model parameters.

| | Parent grain | Twins |
|---|---|---|
| $C_{11}$ (GPa) | 198 | 198 |
| $C_{12}$ (GPa) | 125 | 125 |
| $C_{44}$ (GPa) | 122 | 122 |
| $D$ (μm) | 20 | – |
| $e$ (nm) | – | 20 |
| $r$ | – | 3 |
| $b_{110}$ (nm) | 0.256 | 0.256 |
| $\rho_0$ ($m^{-2}$) | $10^{10}$ | – |
| $\tau_{c0}^{slip}$ (MPa) | 125 | 250 |
| $\beta$ (m) | $2 \times 10^{-9}$ | $0.9 \times 10^{-9}$ |
| $\alpha$ | 0.5 | 0.48 |
| $k$ | 10.2 | 14.5 |
| $\tau_{c0}^{tw}$ (MPa) | 230 | – |
| $H_{cp}$ (MPa) | 5850 | – |
| $H_{ncp}$ (MPa) | 9000 | – |
| $b$ | 0.2 | – |

following Ref. [27]. Uniaxial tension and plane-strain compression were simulated using the crystal plasticity model presented above and the predictions were compared to experimental results at two length scales: the polycrystal level and the grain level.

### 3.1. Macroscopic response in uniaxial tension

Tensile tests were performed along the rolling direction (RD) at a strain rate of $1.8 \times 10^{-4}\,s^{-1}$, at room temperature. Model parameters were calibrated so as to reproduce the macroscopic work hardening and the evolution of the twin volume fraction. Their values are listed in Table 1. Only $\tau_{c0}$, $\beta$, $\alpha$, $k$ and the twinning kinetics parameters $H_{cp}$ and $H_{ncp}$ were considered in the fitting procedure, the other parameters being experimentally measured $(D, e)$ or taken from the literature [11].

Fig. 3a and b depict the experimental and simulated stress–strain curves (until the onset of diffuse necking) and the corresponding incremental hardening coefficient $n_{incr} = \frac{\varepsilon}{\sigma}\frac{\partial \sigma}{\partial \varepsilon}$. For clarity, experimental curves were filtered in order to remove serrations characteristic of dynamic strain aging, as detailed in Ref. [29]. For comparison purpose, the stress–strain curve predicted by the same model but with deformation twinning switched off is also shown.

The rate of deformation twinning (averaged over the polycrystal) was determined from electron backscatter diffraction in a field emission gun scanning electron microscope, with a resolution of 120 nm. In Fig. 4a, corresponding to 10% deformation, the nuclei of deformation twins revealed by transmission electron microscopy (TEM) [21] are hardly observed at the resolution of the EBSD analysis. However, twins (in reality twin bundles [21,23]) are clearly seen after 30% deformation (Fig. 4b). Moreover, such twins are mostly present in ⟨1 1 1⟩//TA (blue[1]) grains (⟨1 1 1⟩ pole aligned with

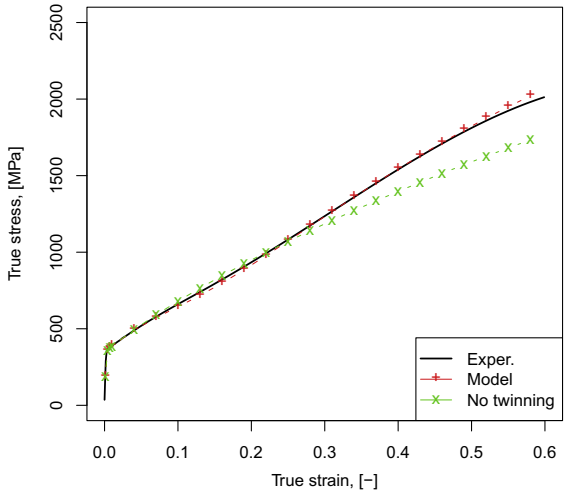


(a) Stress-strain curve

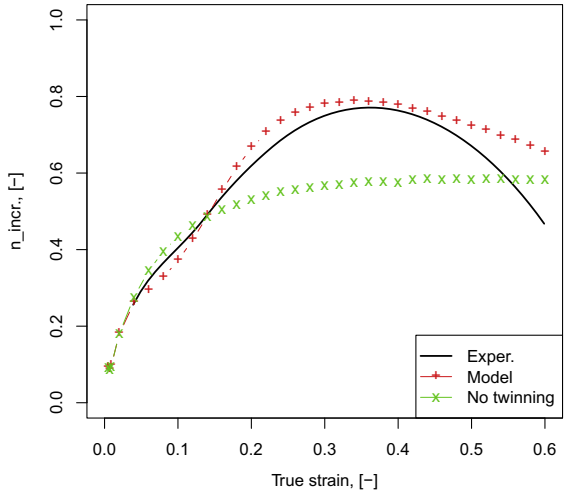


(b) Incremental hardening coefficient, $n_{incr} = \frac{\varepsilon}{\sigma}\frac{\partial \sigma}{\partial \varepsilon}$

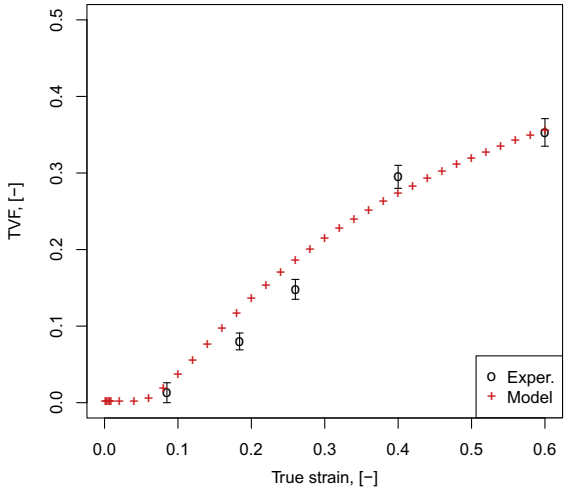


(c) Twin volume fraction (TVF)

Fig. 3. Calibration of the multisite model for work hardening and twin volume fraction in tension.

[1] For interpretation of color in Figs. 1–10, the reader is referred to the web version of this article.

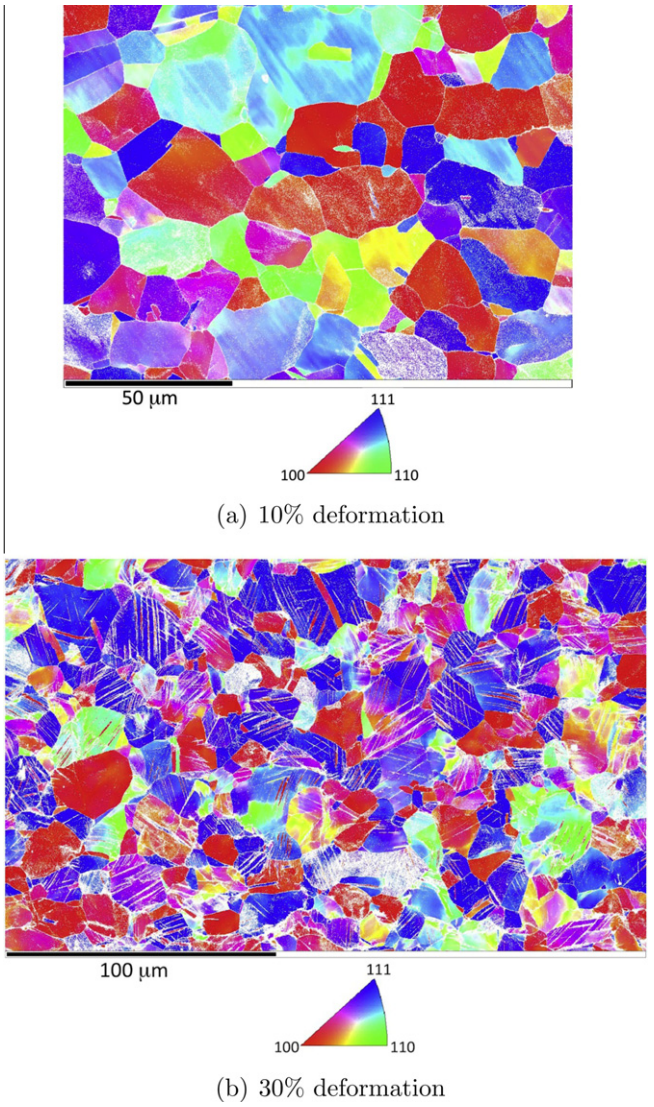


Fig. 4. Tensile axis inverse pole figure (TA-IPF) EBSD maps of the TWIP microstructure in tension.

the tensile axis) and almost absent from grains belonging to the ⟨100⟩//TA (red) crystallographic fiber. This is in accordance with previous observations of various TWIP steels in tension [23,30–33].

The TVF was estimated after different amounts of strain by applying stereology principles after careful counting of the twins inside maps of either the diffraction pattern quality or the inverse pole figure (IPF) relative to the tensile axis [20]. Each measurement was repeated five times to assess the reliability of the method. The experimental and simulated TVF are depicted in Fig. 3c. The onset of twinning (confirmed by TEM analysis) occurs after a few per cent of deformation. The twin volume fraction reaches approximately 35% at maximum uniform elongation.

Texture analysis in the deformed state, i.e. after 30% elongation, was performed by means of XRD in order to assess the development of texture predicted by the model. As already depicted qualitatively by EBSD, the IPF of the experimental texture (Fig. 5a) reveals two crystallographic fibers for which the tensile axis is aligned with ⟨100⟩ and ⟨111⟩, respectively. This trend is reproduced by the model. For comparison purpose, the texture prediction of the multisite model in Fig. 5c is compared to the ones obtained with the Taylor FC model (Fig. 5b, isodeformation assumption) and with CPFEM (Fig. 5d).[2] It can be observed that the Taylor model produces a sharper texture than the experimental one. Allowing strain heterogeneity (multisite model and CPFEM) yields more realistic intensities of the texture components. This is in agreement with former results concerning the assessment of these crystal plasticity models [18,19,34]. The multisite and CPFEM textures are closest to the experimental one. Nevertheless, whereas the experimental IPF exhibits similar intensities at the ⟨100⟩//TA and ⟨111⟩//TA poles (around 2.2), the simulated IPF overestimate the intensity of the ⟨100⟩// TA pole (IPF = 3.0–3.4) compared to the ⟨111⟩//TA pole (IPF = 2.6).

### 3.2. Uniaxial tension of prestrained samples

A more complex deformation path was investigated next, consisting of a prestrain (with maximum equivalent deformation of 40.6%) by cold rolling, followed by uniaxial tension in the transverse direction (TD). This two-step process was simulated with the multisite model by assuming plane-strain compression (PSC) during rolling and by accounting for elastic unloading before the tensile test along TD. The corresponding tensile curves are shown in Fig. 6. This demonstrates the ability of the model to deal with non-monotonic loading paths.

### 3.3. Macroscopic texture development during cold rolling

Texture development after cold rolling down to 54% thickness reduction (0.9 equivalent strain) of the same alloy was predicted using the very same model. The $\phi_2 = 45°$ sections of the ODF presented in Fig. 7 correspond to different assumptions about the micro–macro scale transition. The experimental texture of Fig. 7a is a typical fcc rolling texture [5,34], where the "copper" component ($\{112\}\langle 111\rangle$, i.e. $\phi_1 = 90°$, $\Phi = 35°$, $\phi_2 = 45°$) in Fig. 7a is somewhat lower than the "brass" component ($\{110\}\langle 112\rangle$, i.e. $\phi_1 = 55°$, $\Phi = 90°$, $\phi_2 = 45°$). This conforms to other rolling texture measurements for different TWIP steels [35,36]. Predicted ODFs reproduce the experimental trend with varying accuracy. As in the case of tension, the Taylor FC texture is too sharp both in the copper and in the brass regions. Models allowing strain heterogeneity yield more reliable texture predictions. In particular, CPFEM predicts a larger ODF intensity in the brass (and Goss) region than in the copper region.

[2] Note that the model parameters in Table 1 were refitted in each case in order to retrieve the same experimental work hardening and twin volume fraction.

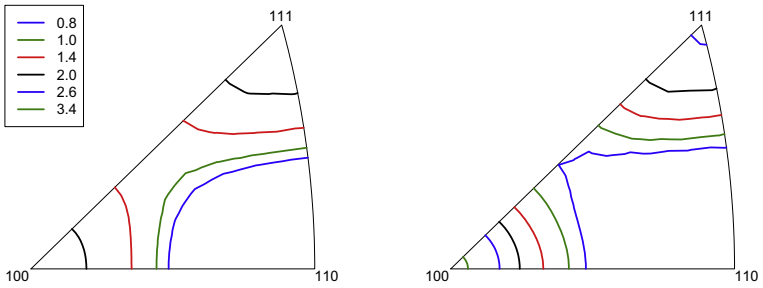


(a) Experimental, X-ray diffraction




(b) Taylor FC

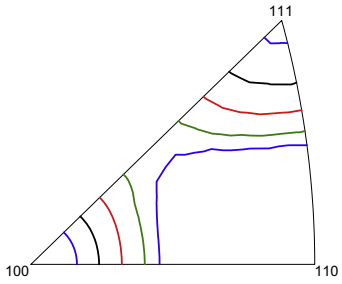


(c) Multisite model

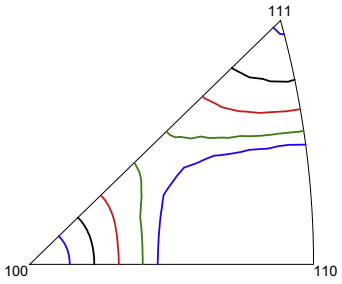


(d) Finite Elements

Fig. 5. Tensile axis inverse pole figures (TA-IPF) of the macroscopic texture at 30% tension.

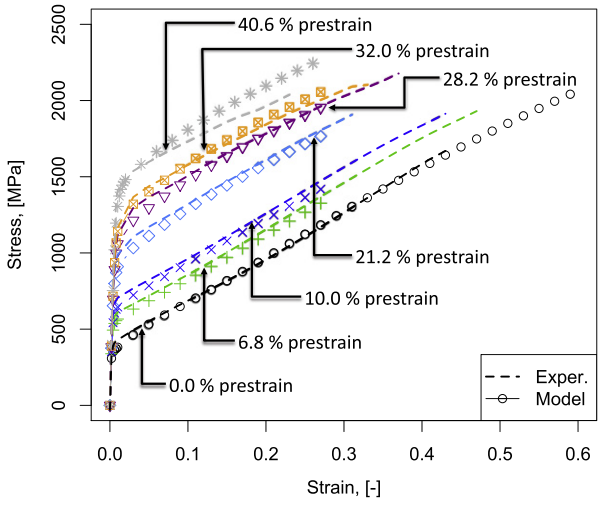


Fig. 6. Experimental and simulated (multisite) tensile curves (transverse direction) after various levels of cold-rolling prestrain.

### 3.4. Model predictions at the grain level

Next, the model was assessed at the grain level, using EBSD data of the 30% deformed tensile specimen. For this, about 50 representative and well-indexed grains were selected in the EBSD map of Fig. 4b. Grains with the same[3] average lattice orientations were identified in the deformed finite-element mesh (containing 1024 grains in total) and were compared one by one to the EBSD data. Note that a model assessment of this type thus involves grains having the same final orientation but a different neighborhood.

In practice, EBSD data was processed as follows. First, each grain was isolated and the average lattice orientation of each entity (parent grain and twin(s)) was computed. Diffraction patterns stemming from twin lamellae have lower quality because the diffraction volume generally includes some of the adjacent untwinned region, especially when the electron beam points to a bundle of very thin twins. According to TEM, the thickness of twin lamellae ranges from 20 to 100 nm for this steel [21]. A consequence is that indexation of the patterns may be impeded in the twins. In contrast, in the parent grains, the diffraction pattern quality is high and all grid points are properly indexed. The local TVF was hence computed considering all pixels with either a twin orientation or a non-indexed pattern. The average rate of indexation was 24% inside the twins. Finally, following the procedure presented in Ref. [37], the orientation spread within each entity of the grain was calculated as the average disorientation of each pixel relative to the average lattice orientation of the entity.

Similar measurements were performed on the grains that were selected in the deformed finite-element mesh. Fig. 8a compares the predicted and experimentally measured TVF in each grain.[4] The lattice orientation of the twins

[3] More exactly, selected simulated grains are disoriented by less than 7° from the experimental ones.

[4] For the model, this corresponds to the average TVF predicted in the 128 integration points forming the grain.

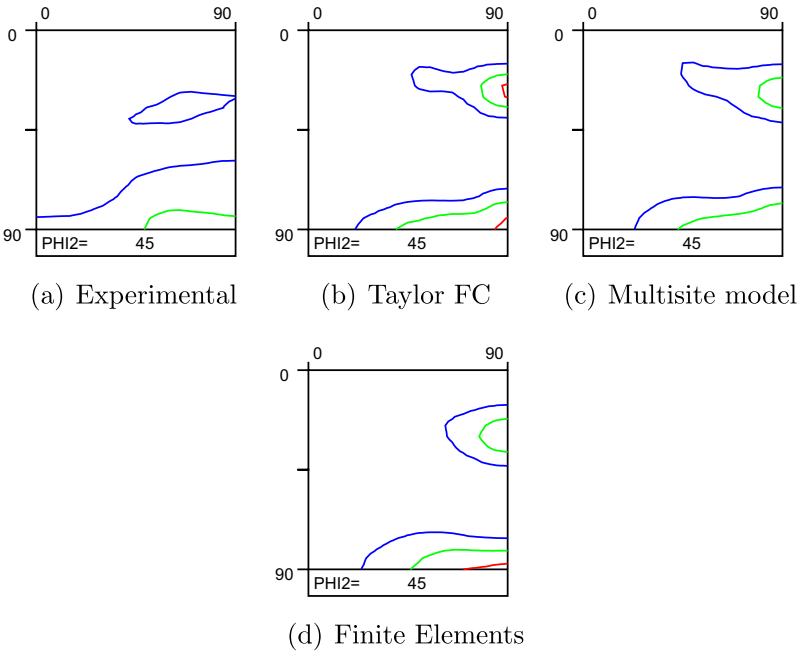


Fig. 7. $\phi_2 = 45°$ Sections of the orientation distribution functions (ODFs) after 54% reduction in cold rolling (TVF around 36% for the models). Contour lines: 1.0, 4.0, 8.0, 12.0. Horizontal axis: $\phi_1$; vertical axis: $\Phi$.

was predicted to within less than 5°, confirming that the model properly identifies the most active twinning plane in each grain. The average orientation spread relative to the mean orientation of the parent grain is shown in Fig. 8b. In these plots, grains are ordered according to their proximity relative to the ⟨1 0 0⟩//TA fiber. If several grains of the finite-element mesh had the same final orientation, only the one showing best agreement with experiment was included in Fig. 8.

The average grain orientation clearly influences the kinetics of twinning. This effect is best seen in Fig. 9a where the position in the IPF indicates the lattice orientation, whereas the symbols identify different amplitudes of the average TVF of each grain. The dotted line divides the IPF into two regions: on the left, the largest Schmid factor is obtained for dislocation slip, whereas, on the right, it corresponds to a twinning system. In reality, the assumption due to Sachs [38], according to which all grains undergo the same stress and activate a single slip or twin system, is incorrect. Nevertheless, the general trend in Fig. 9a is that the TVF of the selected grains is larger on the right of the dotted line. In the EBSD map of Fig. 4b, most of the visible twins are indeed inside ⟨1 1 1⟩//TA (blue) grains.

The model predictions presented in Fig. 9b–d explain why certain grains of the right-hand side region produce much less twins than what is expected from a simple Schmid analysis (and vice versa). The trajectory of a number of grains is shown: a straight line is drawn between the initial and final orientations of the grains, the latter being represented with a marker. This reveals a global reorientation of the grains towards the stable ⟨1 1 1⟩//TA and ⟨1 0 0⟩//TA fibers. The models predict a lower—but not necessarily zero—TVF within grains ending up close to the ⟨1 0 0⟩// TA fiber. Grains with maximum TVF do not belong to the ⟨1 1 1⟩//TA fiber exactly, but rather stem from a region between ⟨1 1 0⟩//TA and ⟨1 1 1⟩//TA.

The simulated IPFs also show to what extent strain heterogeneity throughout the polycrystal influences lattice reorientation (i.e. texture development) and twinning. The Taylor FC model (Fig. 9b) produces regular "stream lines": crystals with nearby initial orientations experience similar reorientations. In the case of the multisite model (Fig. 9c), the interaction of each grain with one neighbor (selected randomly) and the shear relaxation along the interface leads to a more scattered pattern (with regard to both lattice reorientation and twinning kinetics). The predictions of CPFEM in Fig. 9d, where both strain compatibility and stress equilibrium are ensured, lie in between. The ⟨1 1 1⟩//TA and ⟨1 0 0⟩//TA fibers strengthen independently of the model used. The scattered pattern predicted in the presence of local grain interactions (multisite model and CPFEM) is directly responsible for the softer (and more realistic) textures obtained with these models (Figs. 5 and 7), as compared to the Taylor FC predictions.

## 4. Discussion

As compared to other steel grades, TWIP steels exhibit unusual hardening behavior. This phenomenon was addressed here by relying on a crystal plasticity model accounting for the effect of mechanical twinning on both the hardening and the selection of dislocation slip systems, i.e. the anisotropy of individual crystals. Whereas the

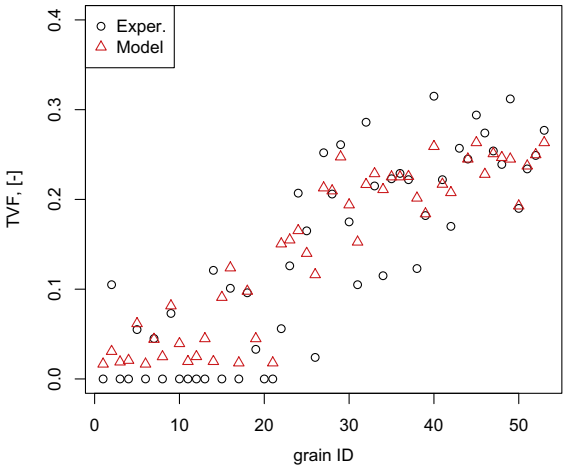


(a) Average twin volume fraction

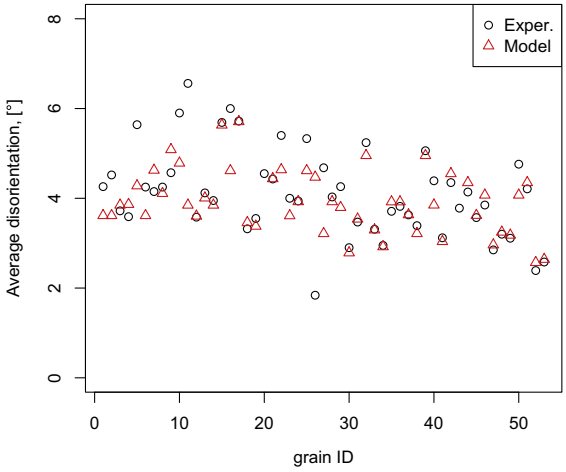


(b) Average disorientation

Fig. 8. Experimental and predicted TVF and disorientation in the parent grains: 30% tension.

macroscopic strengthening can be measured during mechanical tests, the interplay of dislocation slip and twinning is revealed indirectly through the development of texture and the rate of twinning. Thanks to EBSD, both of the latter may be probed at the grain scale. The strategy of the present study has been to fit hardening parameters based on the macroscopic tensile curve and the average rate of twinning measured at the polycrystal level (Fig. 3). Different assumptions about the micro–macro scale transition were then tested, by applying the model to another deformation mode (PSC) and by analyzing texture predictions.

The multisite model proved to constitute a fairly accurate and computationally cheap alternative to CPFEM, at least after moderate strains (30%) in tension. By accounting for local interactions of adjacent grains, both of the latter approaches improve texture predictions as compared to the classical Taylor FC model. CPFEM was most successful after large deformations (54% thickness reduction in rolling). It is likely that the assumption of pairwise interaction with a single adjacent grain (the basis of the multisite model) is satisfactory only under moderate strains. The more intricate deformation patterns expected in highly deformed samples are captured only by CPFEM. Nevertheless, the predictions of rolling textures obtained here are somewhat less accurate than some previous ones [6] that deviate away from the isostrain assumption (Taylor FC) towards the isostress assumption (Sachs). Although the selected hardening law was meant to promote dislocation slip predominantly parallel to the most active twin plane (as recommended in order to capture the copper-to-brass texture transition [5]), none of the scale transition schemes tested here led to single slip inside individual grains. A recent study [34] relying on similar hypotheses has shown that concentration of slip on a single slip plane is not achieved even when the CPFEM mesh is highly refined. We did not predict the so-called "composite deformation pattern" according to which strain heterogeneities due to single slip in heavily twinned grains is accommodated by multislip in the surrounding material. Only about one-third of the grains had their most active slip plane parallel to the main twinning plane. Micro-shear bands may also contribute to the copper-to-brass texture transition [9]. However, plastic localization into shear bands was not observed (neither by EBSD nor by TEM) at the level of deformation considered in this study.

On the other hand, at the level of individual grains, the grain interaction models (multisite and CPFEM) are more successful than the Sachs model. They properly predicted the active twinning mode(s), even in the less favorably oriented grains. A strong effect of grain orientation on the occurrence of twinning is revealed in Fig. 9, in agreement with previous experimental observations [23,30–33]. However, when attempting to explain the amount of twinning observed in a given grain, a simple Schmid analysis does not suffice. The predictions are slightly improved based on the Taylor model which predicts a different stress state inside each grain and which accounts for the fact that twinning may occur early in the deformation process and be followed by a lattice rotation towards a less favorable orientation. Gutierrez-Urrutia et al. [33] highlighted the effect of stress concentration at grain boundaries—due to impinging bundles of twins—as a possible explanation for twin nucleation in neighboring, less favorably oriented grains. The present analysis accounts in a simplified manner for the influence of grain interactions on the stress state inside each grain. Two grains with the same initial orientation will produce different amounts of twins and may also rotate towards different final orientations if they interact with different neighbors. This is illustrated in Fig. 10. Four grains were considered, the first three close to, respectively, the ⟨100⟩//TA, ⟨110⟩//TA and ⟨111⟩//TA fibers, and the last one remote from all others. Using the multisite model repeatedly, each grain was associated successively with 20 randomly selected neighbors. Fig. 10 depicts the grain reorientation and TVF for these four grains. In particular, grains initially in the center of the IPF may be pulled in one

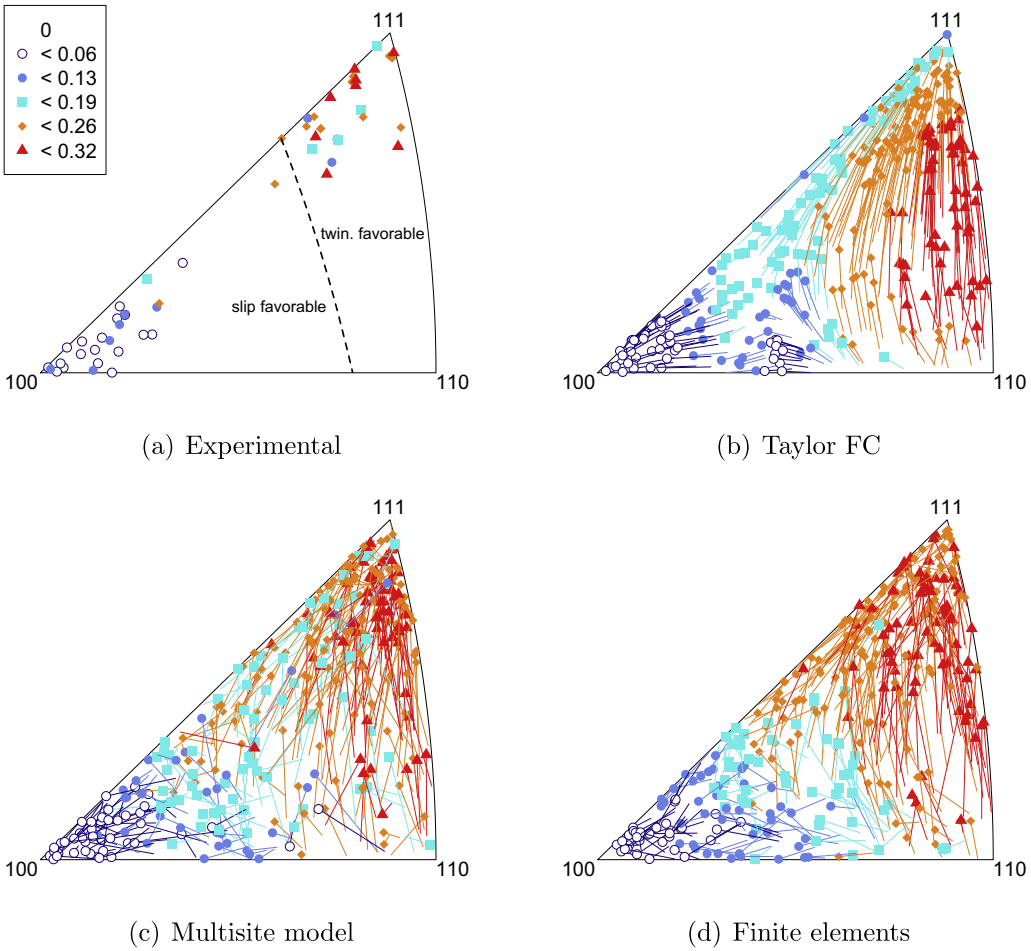


Fig. 9. TA-IPF illustrating the local twin volume fraction and parent grain reorientation at 30% tension. Only 1/3 of the grains are represented in the numerical IPFs for the purpose of clarity. A straight line is drawn between the initial and final orientation of the grains, the latter being highlighted with a marker.

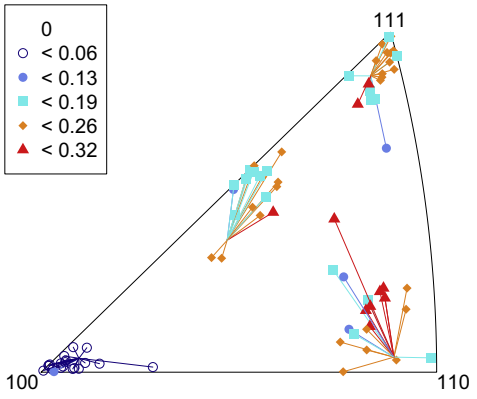


Fig. 10. Influence of the next neighbor interaction on the parent grain reorientation and the twin volume fraction in the multisite model (30% tension). Each of the four initial grains is associated in pairs with 20 random grains.

direction or the other depending on their interactions. Similar trends are expected in 3-D polycrystals, implying interactions of each grain with more than one neighbor.

It is important that predictions of texture development be conducted with a realistic hardening law. Referring to the analysis of work hardening performed by Shiekhelsouk et al. [11] on a similar TWIP material, one can note in Fig. 3b a slight slowdown in the experimental incremental hardening around 0.05–0.10 strain. It corresponds to the onset of twinning, as can be seen in Fig. 3c. According to [11], twinning causes a relaxation before it starts reducing the dislocation MFP. Contrary to the work of Shiekhelsouk et al., the present model captures the decrease in incremental hardening at large strain (above about 0.35), though not as pronounced as in the experiment.

Fig. 3 shows the effect of twinning on the predicted hardening cuve. However, the curve labeled "No twinning" still presents a large work-hardening rate as compared to common fcc steels not subjected to mechanical twinning. Virtual material like this created by switching off twinning in the model probably has a much lower dynamic recovery rate than real materials. Indeed, besides other mechanical consequences explicitly taken into account in the present model, the formation of twins induces storage of dislocations along latent slip planes as a consequence of the

sequence of dislocations reactions that leads to their formation [21]. This implicit contribution to hardening could not be switched off.

Predicting nucleation and growth of twins based on a generalized Schmid law, as was done in the present study, represents strong simplifications compared to reality. Mechanisms of twin formation in TWIP steels have been studied by TEM [21] and are much more intricate than the simple attainment of a threshold shear stress. Gutierrez-Urrutia et al. [33] reported that the initial twinning resistance depends on the grain size. Twin nucleation is typically associated with particular dislocation structures and multiple slip was identified as a necessary condition for its occurrence (e.g. [39]). An improved law for the activation of twinning would hence have to account for the influence of dislocation slip on twin nucleation and twin growth, respectively.

Finally, while mechanical anisotropy was probed here only through the tensile tests on prestrained (rolled) samples, an earlier version model [40] was shown to adequately capture the different trends in work hardening and texture development in simple-shear (free-end torsion) for a brass material. In addition, although the proposed model can, in principle, already address complex strain paths such as cyclic loadings, it is expected that predictions will be unsatisfactory until a distinction is made between isotropic and kinematic hardening. Back-stresses were shown to be significant in TWIP steel [41] and this is only partly explained by the composite type of hardening [13] referred to in the introduction.

## Acknowledgements

L.D. and P.J.J. are supported by the FNRS (Belgium). The study was partly financed through the IAP6-24 project financed by the Belgian Science Policy. Computing facilities were made available through contract FRFC-2.4502.05 with FNRS.

## References

[1] Remy L. Acta Metall 1978;26(3):443–51.
[2] Karaman I, Sehitoglu H, Beaudoin A, Chumlyakov Y, Maier H, Tome C. Acta Mater 2000;48(9):2031–47.
[3] Allain S, Chateau J, Bouaziz O. Mater Sci Eng A 2004;387:143–7.
[4] Bouaziz O, Allain S, Scott C, Cugy P, Barbier D. Curr Opin Solid State Mater Sci 2011;15(4):141–68.
[5] Leffers T, Ray R. Prog Mater Sci 2009;54:351–96.
[6] Leffers T, Lebensohn R. In: Liang Z et al., editors. Proceedings of the 11th ICOTOM. Beijing: International Academic Publishers; 1996. p. 307–14.
[7] Proust G, Tome C, Kaschner G. Acta Mater 2007;55(6):2137–48.
[8] Staroselsky A, Anand L. J Mech Phys Solids 1998;46(4):671–3. 675–696.
[9] Kalidindi S. Int J Plast 2001;17(6):837–60.
[10] Bouaziz O, Guelton N. Mater Sci Eng A 2001;319(Sp. Iss. SI):246–9.
[11] Shiekhelsouk M, Favier V, Inal K, Cherkaoui M. Int J Plast 2009;25(1):105–33.
[12] Beyerlein I, Tome C. Int J Plast 2008;24(5):867–95.
[13] Gil Sevillano J. Scripta Mater 2009;60(5):336–9.
[14] Kalidindi S. J Mech Phys Solids 1998;46:267–90.
[15] Barbe F, Decker L, Jeulin D, Cailletaud G. Int J Plast 2001;17(4):513–36.
[16] Roters F, Eisenlohr P, Hantcherli L, Tjahjanto D, Bieler T, Raabe D. Acta Mater 2010;60:1152–211.
[17] Quey R, Dawson P, Barbe F. Comput Methods Appl Mech Eng 2011;200(17–20):1729–45.
[18] Van Houtte P, Li S, Seefeldt M, Delannay L. Int J Plast 2005;21:589–624.
[19] Delannay L, Melchior M, Signorelli J, Remacle J, Kuwabara T. Comput Mater Sci 2009;45(3):739–43.
[20] Renard K, Jacques PJ. Mater Sci Eng A, accepted for publication, doi:10.1016/j.msea.2012.01.123.
[21] Idrissi H, Renard K, Ryelandt L, Schryvers D, Jacques PJ. Acta Mater 2010;58(7):2464–76.
[22] Hutchinson J. Metall Mater Trans A 1969;8:1465–9.
[23] Barbier D, Gey N, Allain S, Bozzolo N, Humbert M. Mater Sci Eng A 2009;500(1–2):196–206.
[24] Kocks U, Mecking H. Prog Mater Sci 2003;48(3):171–273.
[25] Franciosi P. Acta Metall 1985;33(9):1601–12.
[26] Lebensohn R, Tome C. Acta Metall Mater 1993;41(9):2611–24.
[27] Melchior M, Delannay L. Comput Mater Sci 2006;37(4):557–64.
[28] Delannay L, Jacques PJ, Kalidindi S. Int J Plast 2006;22(10):1879–98.
[29] Renard K, Ryelandt S, Jacques PJ. Mater Sci Eng A 2010;527(12):2969–77.
[30] Yang P, Xie Q, Meng L, Ding H, Tang Z. Scripta Mater 2006;55(7):629–31.
[31] Ueji R, Tsuchida N, Terada D, Tsuji N, Tanaka Y, Takeinura A, et al. Scripta Mater 2008;59:963–6.
[32] Jimenez J, Frommeyer G. Mater Character 2010;61:221–6.
[33] Gutierrez-Urrutia I, Zaefferer S, Raabe D. Mater Sci Eng A 2010;527(15):3552–60.
[34] Melchior M. Modelling of texture and hardening of twip steel – advanced finite element representation of polycrystalline aggregates. Ph.D. thesis, Université Catholique de Louvain, Louvain la Neuve; 2009.
[35] Vercammen S, Blanpain B, De Cooman B, Wollants P. Acta Mater 2004;52(7):2005–12.
[36] Bracke L, Verbeken K, Kestens L, Penning J. Acta Mater 2009;57(5):1512–24.
[37] Delannay L, Mishin O, Jensen D, Van Houtte P. Acta Mater 2001;49(13):2441–51.
[38] Sachs G. Z Verein Deutsch Ing 1928;72:734–6.
[39] Christian J, Mahajan SS. Prog Mater Sci 1995;39(1–2):1–157.
[40] Dancette S, Delannay L, Jodlowski T, Giovanola J. Int J Mater Form 2010;3:251–4.
[41] Bouaziz O, Allain S, Scott C. Scripta Mater 2008;58(6):484–7.